ELECTRON BEAM DIAGNOSTICS FOR FEL STUDIES AT CLARA

S. Spampinati#, University of Liverpool & The Cockcroft Institute, Cheshire, UK
D. Newton, University of Liverpool, Liverpool, UK

Abstract

CLARA (Compact Linear Accelerator for Research and Applications) is a proposed 250 MeV, 100-400 nm FEL test facility at Daresbury Laboratory [1]. The purpose of CLARA is to test and validate new FEL schemes in areas such as ultra-short pulse generation, temporal coherence and pulse-tailoring. Some of the schemes that can be tested at CLARA depend on a manipulation of the electron beam properties with characteristic scales shorter than the electron beam. In this article we describe the electron beam diagnostics required to carry on these experiments and simulations of FEL pulse and electron beam measurements.

INTRUDUCTION

Some of the most advanced schemes proposed to improve FEL performance depend on a manipulation of the electron beam properties with characteristic scales of several coherence lengths and shorter than the electron beam [2-4]. We are interested to test, among other schemes, mode locking FEL and femto-slicing for the production of trains of short pulses [4-7]. The implementation of these schemes at CLARA requires a 30 - 50 μm modulation of the beam energy acquired via the interaction with an infrared laser beam in a short undulator (modulator). The performance of these FEL schemes depends on this energy modulation. So monitoring the longitudinal phase space of the electron beam is important to perform and to realize these experiments. A deflecting cavity [8] installed in the last part of the FEL line will allow the longitudinal beam distribution to be observed on a screen placed after the dipole leading to the beam dump. The FEL line of CLARA, as shown in Fig. 1a, is composed of two modulators separated by a dispersive section, seventeen radiators and an afterburner section. The afterburner is composed by a series of short undulators and delay chicanes. A possible layout of the diagnostic system placed at the end of the CLARA undulator from the afterburner is shown in Fig. 1b.

In this design, the electron beam is deflected vertically by the deflecting cavity. This deflection maps the electron beam longitudinal coordinate to the vertical coordinate on an intercepting screen after the spectrometer dipole magnet; the dipole converts the particle's energy to the screen horizontal coordinate. Consequently, the electron beam longitudinal phase space is imaged on the screen, and the energy modulation taking place in the modulator can be studied and optimized. Another interesting application of this diagnostic beam line could be the study of the FEL process taking place in the different operation modes of CLARA.

#simone.spampinati@cockcroft.ac.uk

ISBN 978-3-95450-134-2

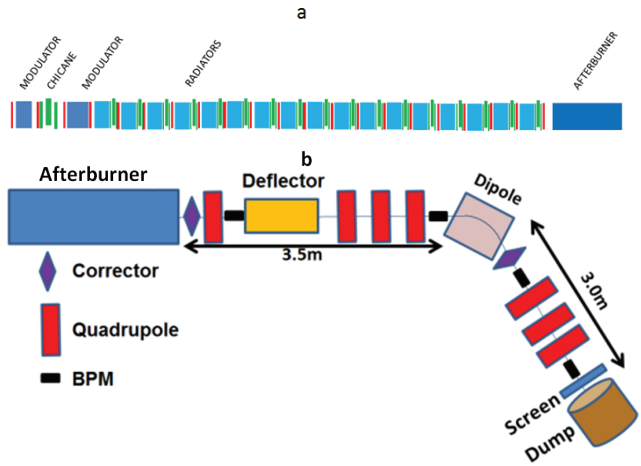

Figure 1: Top: FEl line of CLARA. Bottom: Layout of the phase space diagnostics composed by of a transverse deflector and an energy spectrometer.

OPTICS OPTIMIZATION AND RESOLUTIONS

The vertical beam size at the screen, after deflection, is [9]:

$$\sigma_y = \sqrt{\sigma_{y,0}^{\ 2} + (S\sigma_Z)^2} \tag{1}$$

where $\sigma_{y,0}$ the vertical beam size at the screen location without deflection is, σ_z is the longitudinal beam size and S is the calibration factor representing the strength of the beam deflection [9]:

$$S = \frac{e_0 V k}{pc}\sqrt{\beta_{yS}\beta_{yD}}\left|\sin\Delta\Psi\right| \tag{2}$$

here $k = \frac{2\pi}{\lambda}$ with λ = 10.01cm for an S-band cavity (frequency of 2.998 GHz). V_0 is the deflecting voltage, $\beta_{y,D}$ and $\beta_{y,S}$ are vertical betatron functions at the deflector and the screen, respectively. ΔΨ is the vertical betatron phase advance between the deflector and the screen. The size of the image of the beam detected on the screen will be increased by the system resolution (screen and CCD pixel size) and:

$$\sigma_y = \sqrt{\sigma_{y,0}^{\ 2} + \sigma_{screen}^{\ 2} + (S\sigma_Z)^2} \tag{3}$$

where σ_{Screen} is the screen and CCD resolution.

The longitudinal resolution of the screen image, $\sigma_{L,r}$ can be defined as the ratio of the non-deflected beam size on the screen to the calibration factor S [10]:

$$\sigma_{L,r} = \frac{pc}{e_0 V k \left|\sin\Delta\Psi\right|}\sqrt{\frac{\varepsilon_n}{\gamma\beta_{yD}} + \frac{(\sigma_{screen})^2}{\beta_{yS}\beta_{yD}}} \qquad (4)$$

The third term in Eq. 3 is equal to the quadratic sum of first two terms for $\sigma_z = \sigma_{L,r}$. The energy resolution of the spectrometer can be written as [10]:

$$\sigma_E = \sqrt{\frac{E^2}{\eta^2}\frac{\varepsilon_n\beta_x}{\gamma} + \frac{E^2}{\eta^2}(\sigma_{screen})^2 + (e_o V k)^2 \frac{\beta_y\varepsilon_n}{\gamma}} \qquad (5)$$

Here η is the horizontal dispersion at the screen. The first two terms represent the resolution of an energy spectrometer line, the third term is the energy spread induced by the deflector [11].

Equations 4 and 5 guide the optimization of the optics functions in the diagnostic beam line. The optimum phase advance between the deflector and the screen is $\Delta\psi = 90^\circ$. Large values of V and $\beta_{y,D}$ lead to a good longitudinal resolution but increase the energy resolution of the system via the induced energy spread. A large value of $\beta_{y,S}$ improves the total longitudinal resolution for a poor resolution screen but has to be narrowed to limit the total beam dimension on the screen given by Eq. 1. A small value of $\beta_{x,S}$ and a large value of η are required to have a good energy resolution.

STUDY OF BEAM ENERGY MODULATION

Figure 2 shows a possible optical solution, used to study the energy modulation (with a spatial period in the range 30-50 μm), from the entrance of the modulator to the screen. The radiators are at maximum gap and the intra-undulator quadrupoles are used along with the seven quadrupoles shown in Fig. 1 to give the required resolution. The optics shown is for beam energy of 150 MeV. The vertical betatron functions at the deflector and at the screen are 25 m and 0.95 m respectively. The calibration factor S, for a deflecting peak voltage of 5 MV and a RF frequency of 2.998 GHz, is ~10.2. The vertical rms beam size on the screen is 2.7 mm. The horizontal betatron function and dispersion at the screen are 1 m and 0.6 m. A longitudinal resolution of 4.7 μm and an energy resolution of 75 Kev are therefore achieved. A screen resolution of 20 μm is assumed. Similar optics and performances can be reached for beam energy of 250 MeV with a deflecting voltage of 7.5 MeV.

The reconstruction of the phase space requires short portions of the bunch to be resolved at the screen. An estimate of the length of these portions of the bunch, that

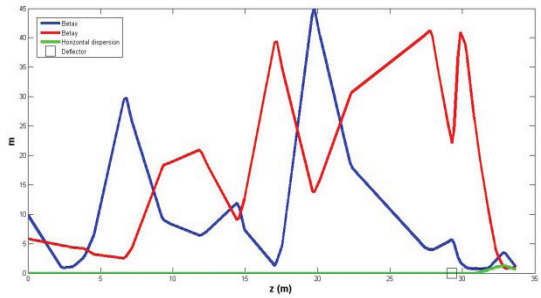

Figure 2: Possible optics from the exit of the modulator to the screen.

can be resolved, can be obtained by using the following simple approach [1, 12]: A portion of the longitudinal density distribution is modelled by two identical Gaussians with different centres in the bunch at a distance Δz. The sigma of the two Gaussians is σ_{screen} /s. This longitudinal test density distribution is reproduced in Fig. 3a. At the screen the separation between the two Gaussian is S·Δz while the sigma is $\sqrt{(\sigma_{y,0})^2 + (\sigma_{screen})^2}$. The vertical profile of the image on the screen is reproduced in Fig. 3b.

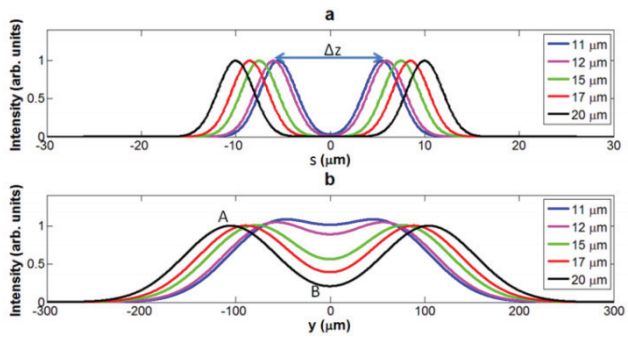

Figure 3: Top: Test longitudinal distributions represented by two Gaussians with a sigma of σ_{Screen} /S separated by a distance Δz. Bottom: Vertical profile on the screen for the distribution depicted above. A and B indicate respectively the values of the intensity of the peaks (the crests) and of the central local minimum (the valley) for any profile.

Simulations including the beam energy modulation in the modulator, the vertical deflection in the RF deflector and the beam transport up to the screen have been performed with the code ELEGANT [13] to test the performance of the diagnostic system introduced above. The parameters used in the simulations are listed in Table 1 and are taken from the CLARA CDR [1]. One-dimensional longitudinal space charge (LSC) and coherent synchrotron radiation (CSR) impedances are included in the simulations.

ISBN 978-3-95450-134-2

Table 1: Simulation Parameters

Parameter	Value	Unit
Macro-particles	2 10^6	
Beam energy	150	MeV
Current	150	A
Energy spread	50 (RMS)	Kev
Emittance	0.6 (RMS)	mm-mrad
Laser wavelength	40	μm
Laser pulse duration	500 (FWM)	fs
Laser pulse energy	10	μJ
Laser waist	2.5	mm
Deflecting frequency	2.998	GHz
Deflecting voltage	5	MV
Screen resolution	20 (RMS)	μm

Results of simulation are shown in Fig. 4. Figure 4a shows the phase space after the interaction in the modulator (see Fig. 1) with the 40 μm laser. Figure 4b shows the beam density distribution projected on the x-y plane at the end of the diagnostic beam line and it representing the screen image. The energy modulation is well evident as predicted above.

We can now compere the beam energy modulation after the laser-electron interaction with the measurements on the screen. We can derive the beam energy modulation on the screen image by using the theoretical value of the calibration factor S (Eq. 2) and of the horizontal dispersion at the screen location. Linear correlated energy spread induced by the deflector, LSC and CSR can be removed. The result is shown in Fig. 5 where the mean slice energy is plotted versus the slice longitudinal coordinate in the bunch. The red curve is the beam energy modulation derived by screen analysis (Fig. 4b) and the blue is the energy modulation present on the beam after the laser-electron interaction in the modulator (Fig. 4a). The agreement between the two curves is good.

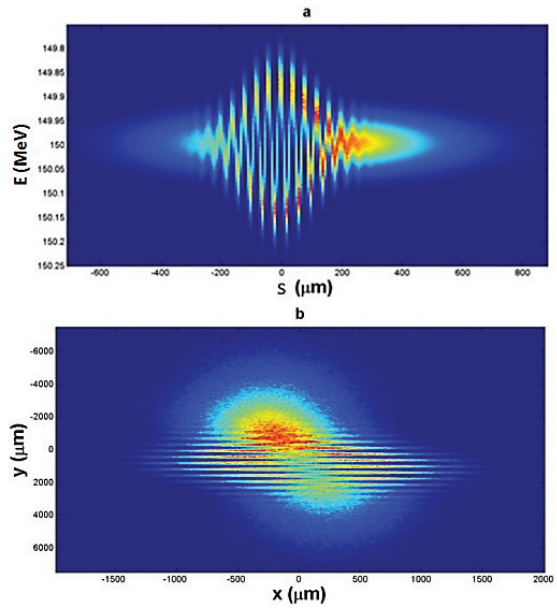

Figure 4: Top: Beam phase space after the interaction in the modulator (see Fig. 1) with the laser. Bottom: beam density distribution projected on the x-y plane at the end of the diagnostic beam line.

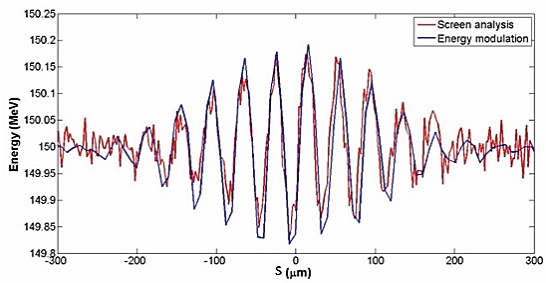

Figure 5: Beam energy modulation derived by the measurement analysis (red) compared with the one gained in the modulator (blue).

STUDY OF THE FEL INTERACTION AND FEL PULSE

Recently a method to study FEL pulse length and fel intensity using a defector and an electron beam spectrometer has been proposed and applied to LCLS experiments [14, 15]. The beam phase space is measured with the FEL on and the FEL off. The application of the energy conservation principle permits to measure the temporal profile of the FEL pulse (E. vs t.) from the changes in the slice mean energy and energy spread induced by the lasing.

The diagnostics described above can be used to study the electron beam phase space with the FEL process on and off to apply this method. In this case the radiators are closed and the intra-radiator qudrupoles are set to ensure beta values required by FEL. We can use the quadrupoles placed after the last radiator to optimize the diagnostics resolutions according to Eq. 4 and Eq. 5. A quadrpupole in the middle of the afterburner has been considered in this case. A possible solution for the optics between the last radiator and the spectrometer screen is shown in Fig. 6. The vertical betatron functions at the deflector and at the screen are 19 m and 0.95 m respectively. The calibration factor S, for a defecting voltage of 5 MV and a RF frequency of 2.998 GHz, is ~9.2. The horizontal beta and dispersion at the screen are 1m and 0.6 m.

ISBN 978-3-95450-134-2

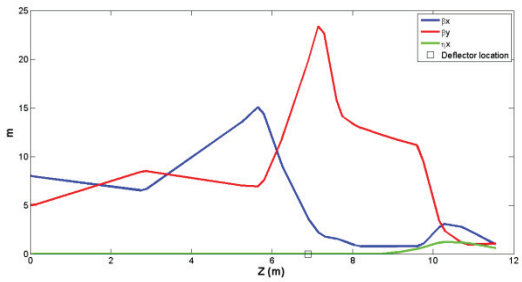

Figure 6: Possible optics from the exit of last radiator to the screen.

For this solution a longitudinal resolution of 5.2 μm and an energy resolution of 63 Kev are predicted by Equations 4 and 5.

As example we consider now the application of the technique described in [9, 14] and demonstrated in [15] to a single stage HGHG. The FEL process is simulated with GENESIS [16] and then the diagnostic line is simulated in ELEGANT as in example described above. In this case the first modulator is tuned at 800 nm to be resonant to a Ti:Sa laser and the radiator is tuned on the fourth harmonic of the seed laser (200 nm). In this case the electron beam has a peak current of 400 A, all the other parameters have the same values as in the previous case. The phase space after the modulator (reconstructed by the image on the diagnostic screen) is reproduced in Fig. 7a. The net energy exchange in this part of the HGHG scheme is negligible. The energy spread is increased on the part of the beam interacting with the laser while the central energy is not modified by the seed. Figure 7b reproduces the phase space after the radiator (5 modules). Radiation production in this stage implies that the beam energy is reduced while the FEL energy is increased. From the two measurements we can determine the slice energy loss induced from the FEL interaction:

$$\Delta E_{FEL}(t) = E_{FEL_{on}}(t) - E_{FEL_{off}}(t)$$

With the obtained time-sliced energy loss and current, laser profile is determined:

$$P_{FEL}(t) = \Delta E_{FEL}(t) \times I(t)$$

The FEL profile reconstructed from the energy loss is shown in Fig. 8 (blue curve) with the profile obtained by the simulation with GENESIS (red curve). The agreement between the two curves is good and in line with the predicted temporal and energy resolution of 15 fs and 10 MW respectively. The pulse duration (rms) of the reconstructed pulse is 55 fs while the simulated pulse has time duration of 66 fs (rms).

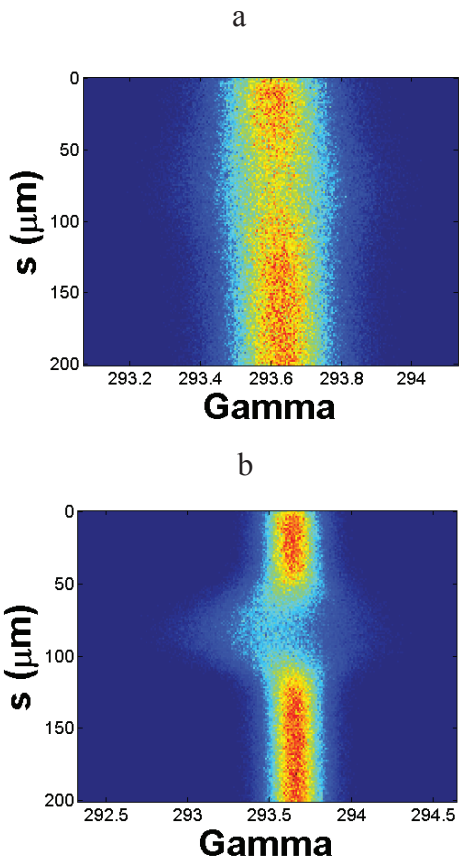

Figure 7: Electron beam phase space after the modulator (a) and after the first five modules of the radiator (b).

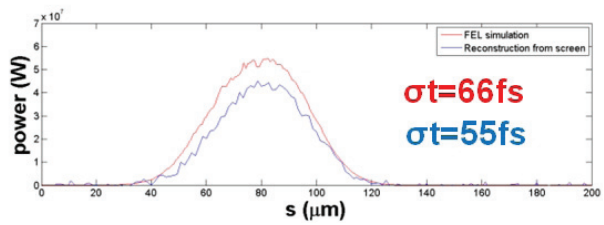

Figure 8: FEL profile as obtained by the simulation with GENESIS and by the screen image.

CONCLUSIONS

We have presented results on the viability of post-FEL diagnostics on CLARA to study the phase space of the beam after the beam energy modulation required by mode locking and sliced FEL schemes. Their expected performance and simulations of their utilization have been presented.

ACKNOWLEDGMENT

This work is funded by STFC (Science and Technology Facilities Council, UK).

ISBN 978-3-95450-134-2

REFERENCES

[1] J. A. Clarke et al., JINST 9, 05 (2014).
[2] A.A. Zholents, W.M. Fawley, Phys. Rev, Lett. 92, 224801 (2004).
[3] E. Kur, D.J. Dunning, B.W.J. McNeil, J. Wurtele & A.A. Zholents, New J. Phys. 13 063012 (2011).
[4] D.J. Dunning, B.W.J. McNeil and N.R. Thompson, Phys. Rev. Lett. 110, 104801 (2013).
[5] E.L. Saldin, E.A. Schneidmiller and M.V. Yurkov, Phys. Rev. ST Accel. Beams 9, 050702 (2006).
[6] N. R. Thompson and B.W.J. McNeil, Phys. Rev. Lett. 100,203901 (2008).
[7] L. Giannessi et al., Phys. Rev. Lett. 106 ,144801 (2011).
[8] G. A. Loew, O.H. Altenmueller, SLAC, PUB-135. Aug. 1965.
[9] Y. Ding et al., "Ultra-short electron bunch and X-ray temporal diagnostics with an x-band transverse deflecting cavity", in: Proc. 1st Int. Beam Instrumentation Conf., Tsukuba, Japan, 2012, TUPA41.
[10] Y. Ding et al., "Commissioning of the X-band Transverse Deflector for Femtosecond Electron / X-Ray Pulse Length Measurements at LCLS", in: Proc. 4th Int. Particle Accelerator Conf., Shanghai, 2013, WEOBB201.
[11] M. Cornacchia and P. Emma, Phys. Rev. ST Accel. Beams 5, 084001 (2002).
[12] P. Craievich et al., "A transverse RF deflecting cavity for FERMI@elettra project", in: Proc. 8th European Workshop on Beam Diagnostics and Int. for Particle Accelerator Conf., Venice, 2007, TUPC10.
[13] M. Borland, ANL/APS Report No. LS-287 (2000).
[14] Y. Ding et al., Phys. Rev. ST Accel. Beams 14, 120701 (2011).
[15] C. Behrens at al. Nature communications 5, 3762 (2014).
[16] S. Reiche et al., Nucl. Instrum. Methods Phys. Res., Sect. A 429, 243 (1999).

ISBN 978-3-95450-134-2